Title: A phenomenological rate of injection model for predicting fuel injection with application to mixture formation in light-duty diesel engines

Authors: Federico Perini*, Wisconsin Engine Research Consultants LLC, Madison, WI
Stephen Busch, Sandia National Laboratories, Livermore, CA
Rolf Deneys Reitz, Wisconsin Engine Research Consultants, LLC, Madison, WI

*corresponding author. E-mail address: Federico.Perini@w-erc.com

Abstract

Fuel injection rate laws are one of the most important pieces of information needed when modeling engine combustion with computational fluid dynamics. In this study, a simple phenomenological model of a common-rail injector was developed and calibrated for the Bosch CRI2.2 platform. The model requires three tunable parameter fits, making it relatively easy to calibrate and suitable for injector modeling when high-fidelity information about the internal injector's geometry and electrical circuit details are not available. Each injection pulse is modeled as a sequence of up to four stages: an injection needle mechanical opening transient; a full-lift viscous flow inertial transient; a Bernoulli steady-state stage, and a needle descent transient. Parameters for each stage are obtained as polynomial fits from measured injection rate properties. The model enforces total injected mass, and the intermediate stages are only introduced if the injection pulse duration is long enough. Experimental rates of injection from two separate campaigns on the same injector were used to calibrate the model. The model was first validated against measured injection rate laws featuring pilot injections, short partially-premixed combustion (PPC) pulses and conventional diesel combustion (CDC) injection strategies. Then, it was employed as an input to engine CFD simulations, which were run to simulate experiments of mixture formation in an optically-accessible light-duty diesel engine. It was found that, though simple, this model is capable of predicting both pilot and main injection pulse mass flow rates well: the simulations yielded accurate predictions of in-cylinder equivalence ratio distributions from injection strategies for both partially-premixed combustion and pilot injections. Also, once calibrated, the model produced appropriate results for a wide range of injected mass and rail pressure values. Finally, it was observed that usage of such a relatively simple model can be a good choice when high-fidelity injection rate input and highly detailed information of the injector's geometry and operation is not available, particularly as noticeable discrepancies can be present also among different experimental campaigns on similar hardware.

Introduction

Direct injection of liquid fuel inside the combustion chamber has allowed significant improvement of indicated efficiency in both diesel engines and, recently, also spark ignition engines, thanks to its ability to generate nearly-stoichiometric, locally ignitable mixtures in-cylinder while keeping the global equivalence ratio low [1, 2]. In diesel engines, advanced fuel injection strategies are the most important control knob to achieving low-temperature and other advanced combustion modes, which are enabled by creating optimal reactivity gradients inside the combustion chamber [3]. Computational fluid dynamics (CFD) models of internal combustion engines require an injection rate law as input, i.e., a time-dependent profile of injected liquid fuel velocity or mass flow rate, for each injection pulse [4]. This is one of the most important parameters to describe the spray behavior, as it affects liquid atomization as well as the fuel/air jet structure [5]. Hence, research on injection system behavior and its modeling is a very active research topic in the engine community.

Two approaches for modeling high-pressure fuel injection can be found in recent literature. The first one aims at capturing fuel injection behavior with high-fidelity modeling of the injector geometry. Advanced experimental techniques such as X-ray tomography are employed to capture flow streamlines, effective flow discharge and non-trivial behavior such as cavitation and dribble [6, 7, 8, 9, 10], and are used to capture fuel injection behavior via high-fidelity Eulerian CFD simulations. For example, Xue et al. have coupled a Eulerian internal nozzle flow simulation with a Lagrangian spray model to produce a high-fidelity initialization of the spray injection rate law and discharge parameters [11]. Vujanovic et al. [12] instead proposed an embedded Eulerian-Eulerian vs. Eulerian-Lagrangian approach, which runs the liquid core simulation as a full Eulerian approach, and then switches to Lagrangian drop generation whenever drops are being detached from the liquid column.

Despite advances in these high-fidelity simulation approaches, the Lagrangian-Drop/Eulerian-Fluid method, initialized by suitable injection rate law and drop size parameters, is still the most widely employed for engine combustion simulations due to the good tradeoff between accuracy and CPU time requirement [13]. Advanced models, such as the one proposed by Bianchi et al. [14], require detailed information about the internal nozzle geometry. For cases when this information is not available, Payri et al. [15] proposed a zero-dimensional injector model suitable for a common-rail system, which employs analytical expressions and correlations fitted to experimental data, to produce reliable injection rates, also including the effects of wear. With a similar approach [16], the same group also proposed a model for the Delphi gasoline injector employed in the Engine Combustion Network's Spray G experiments. Soriano et al. [17] developed a similar injection modeling approach, also adding characteristics of the injector's electric circuitry, such that the rate of injection (ROI) could be predicted starting from the energization signal usually available during engine control diagnostics. Xu et al. [18] also developed a diesel injector model based on polynomial fits on a large experimental dataset and employed it to model partially-premixed combustion in a light-duty diesel engine.

In this work, a model belonging to the second class of injection modeling methods is presented and calibrated for a Bosch CRI2.2 platform injector, whose details are summarized in Table 1. In our approach, no information about internal nozzle geometry or electrical circuitry parameters are needed in order to model rates of injection. Instead, we developed a phenomenological model, based on fitting against a limited number of experimental rate of injection traces only, to support the most common conditions for applications to diesel engine combustion modeling, where such detailed information is likely not available. The paper is structured as follows. First, the stages identified to describe an injection pulse and their equations are described, and the overall solution procedure is presented. Then, the experimental calibration and injection rate validation is shown. Finally, the model is applied to predict in-cylinder air-fuel mixture equivalence ratio measurements with several injection strategies in the Sandia single-cylinder optical light-duty diesel engine. The proposed model is shown to predict both pilot and large injection pulses ROIs well, even if based on relatively few calibration coefficients. Appropriate response to changes in injected mass and rail pressure values is seen. Finally, accurate in-cylinder mixture equivalence ratio predictions were observed. The results overall suggested that such a relatively simple model can be used with success highly detailed information of the injector's geometry and operation is not available: for example, time-resolved needle lift laws are hard to measure, because of ballistic behavior; furthermore, noticeable discrepancies can be present also among different experimental campaigns when employing standard hardware.

Model description

The black-box model was developed to provide an injection pulse's mass flow rate and velocity table given a few details of the injector geometry. Injector geometry is described via the nozzle orifice diameter, d_{noz}, and number of nozzle holes, n_{noz}. Outflow from the injector is described assuming constant fuel liquid density, ρ_f, and given rail pressure, p_{rail}. Assumptions are made for the cylinder's backpressure, (default $p_{cyl} = 50\ bar$), as

Sac volume [mm^3]	0.23
Number of holes	7
Included angle [deg]	149
Nozzle diameter [mm]	0.14
Hole protrusion [mm]	0.3
Injector tip protrusion [mm]	2.1

Table 1. Bosch CRI2.2 Injector properties

well as the orifice's discharge coefficient (assumed $c_D = 0.8$). To compute an injection pulse profile, the only additional input needed is the injected mass amount, m_{inj}.

Each injection pulse is represented as a sequence of up to four separate stages, as represented in Figure 1:

1. the first stage models fuel injection during the needle lift's mechanical transient;
2. second, the hydraulic transient at full needle lift;
3. third, the near-steady-state injection at full lift and maximum injection velocity;
4. fourth, the needle descent phase.

Each stage is linked to the next one using a suitable common boundary injection velocity. Stage priority is 1-4-2-3. Stages 1 and 4 are mandatorily present in each injection pulse, i.e., only needle lift and descent are present if it is short enough. If phase 1 is complete sooner, stage 2 is added. Stage 3 is also added if stage two reaches the maximum injection velocity; it can be arbitrarily extended in time to match the actual injected mass. Each stage's physics are described as follows.

Mechanical needle lift transient. Initial outflow from the injector nozzle is defined by the electro-mechanical needle lift transient. The needle is initially moved by the electromagnetic force impressed by the control circuit, allowing the orifice to open [19]. The nozzle spring undergoes compression as the needle is moving in the opening direction. The instantaneous flow rate is soon governed by both the rate law of orifice area opening, and by the viscous forces and turbulent eddies defining initial fluid motion inside the injector's internal geometry [20, 21]. This initial transient is assumed to be dominated by the area opening effect, hence a parabolic injection rate law behavior is imposed in stage 1, up to a pressure-dependent peak opening velocity:

$$u_{inj}(t \leq \Delta t_1) = c_1(p_{rail}) \cdot t^2 \,. \qquad (1)$$

Based on the experimental measurements later described, total duration of the electromechanical transient is assumed to be a fixed injector property, at $\Delta t_1 = 0.1\, ms$. Hence, the velocity at the end of stage 1 is used as a parameter instead:

$$u_1 = f(p_{rail}) = u_{inj}(\mathrm{p}_{rail}, \Delta t_1). \qquad (2)$$

Hydraulic transient at full lift. The second injection stage starts with the needle lift assumed in steady full-lift position, and it represents the injection velocity transient that the flow field needs to reach steady state after the injector has reached the fully-open mechanical configuration, or when its opening is large enough that the instantaneous flow rate is limited by the fluid's inertial behavior. This stage is dominated by viscous forces, turbulent eddies and potential onset of cavitation inside the nozzle [6, 22]. It is described by a linear velocity increase as follows:

$$u_{inj}(t_1 \le t \le t_2) = u_1 + a_2(p_{rail}) \cdot (t - t_1). \quad (3)$$

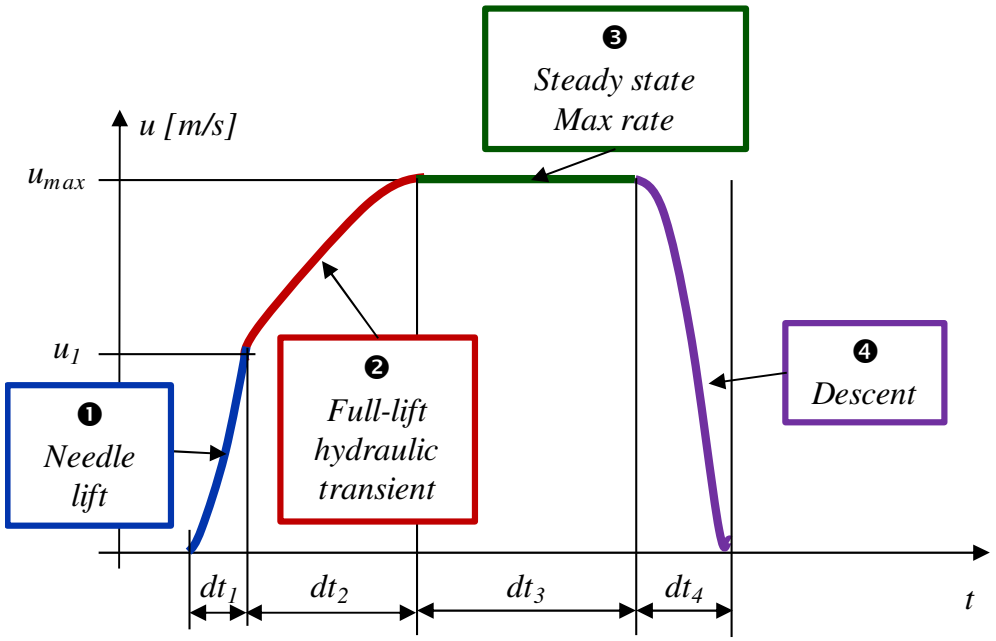

Figure 1. Injection rate stages according to the current model.

Based on this assumption, the time at which the injected flow will reach peak outflow velocity is known:

$$\Delta t_2 = \frac{u_{max} - u_1}{a_2(p_{rail})}. \quad (4)$$

Steady-state maximum rate. The maximum steady-state flow velocity is computed from the Bernoulli equation:

$$u_{max} = C_v \sqrt{2 \frac{p_{rail} - p_{cyl}}{\rho_f}}, \quad (5)$$

where C_v is a velocity coefficient assumed to be constant $C_v = 0.98$ [5]. In the current study, the cylinder pressure $p_{cyl} = 50bar$ is assumed to be constant, similar to the near-TDC pressure in slightly-boosted operation of light-duty diesel engines [23]. If needed, it can be replaced with a more accurate estimation from a motoring engine cycle simulation; however, it is more than one order of magnitude smaller than typical diesel common rail injection pressures in the range $500bar \le p_{rail} \le 2000bar$, so it will have a minor effect on predicted peak velocity.

Needle descent. The final stage models needle descent after the injector's solenoid is not being energized anymore. The dynamics of flow rate reduction are affected by both the mechanical

properties of the injector, such as spring elasticity, as well as viscous forces inside the high-pressure compressible liquid fuel. This stage was described with a linear velocity descent law:

$$u_{inj}(t > t_3) = u_{max} + a_4(p_{rail}) \cdot (t - t_3), \quad (6)$$

where the descent rate, $a_4 < 0$, can be measured from the total descent time:

$$a_4 = -\frac{u_{max}}{\Delta t_4}. \quad (7)$$

Solution procedure.

An injection rate law is generated based on a total injected mass input. The relationship between instantaneous injection velocity and mass flow rate is given by mass conservation through the effective nozzle area:

$$\dot{m}_{inj}(t) = C_D \rho_f A_{noz} u_{inj}(t), \quad (8)$$

where $A_{noz} = n_{noz}\pi d_{noz}^2/4$ represents the total geometric orifice area, and $C_D = 0.8$ the discharge coefficient. This is a reasonable approximation for a simple model as the discharge coefficient is known to vary with the flow Reynolds number at the nozzle diameter, with a limit $Re_D \to \infty$ close to $C_D = 0.8$ [18]; and with relevant deviations only for small Reynolds numbers.

Figure 2 reports an outline of the iterative solution procedure employed to achieve an injection rate matching the desired total mass. First, durations of each injection stage are guessed: stages 1, 2 and 4 are assumed to have full extent, which is defined by velocities u_1 and u_{max} as well as by duration Δt_1. Stage 3 is also assumed to inject the whole mass m_{inj} itself. Then, the injection velocity profile guess is built and the corresponding injected mass is computed as:

$$m_{tot} = \int_{t=0}^{t=\Delta t_1+\Delta t_2+\Delta t_3+\Delta t_4} C_D \rho_f A_{noz} u_{inj}(t)\, dt \quad . \quad (9)$$

The simulated injected mass is iteratively compared with the desired (e.g., measured) value. The initial choice of stage durations always provides greater mass, $m_{tot} \geq m_{inj}$. Excess mass is iteratively removed from the stages, following the priority order.

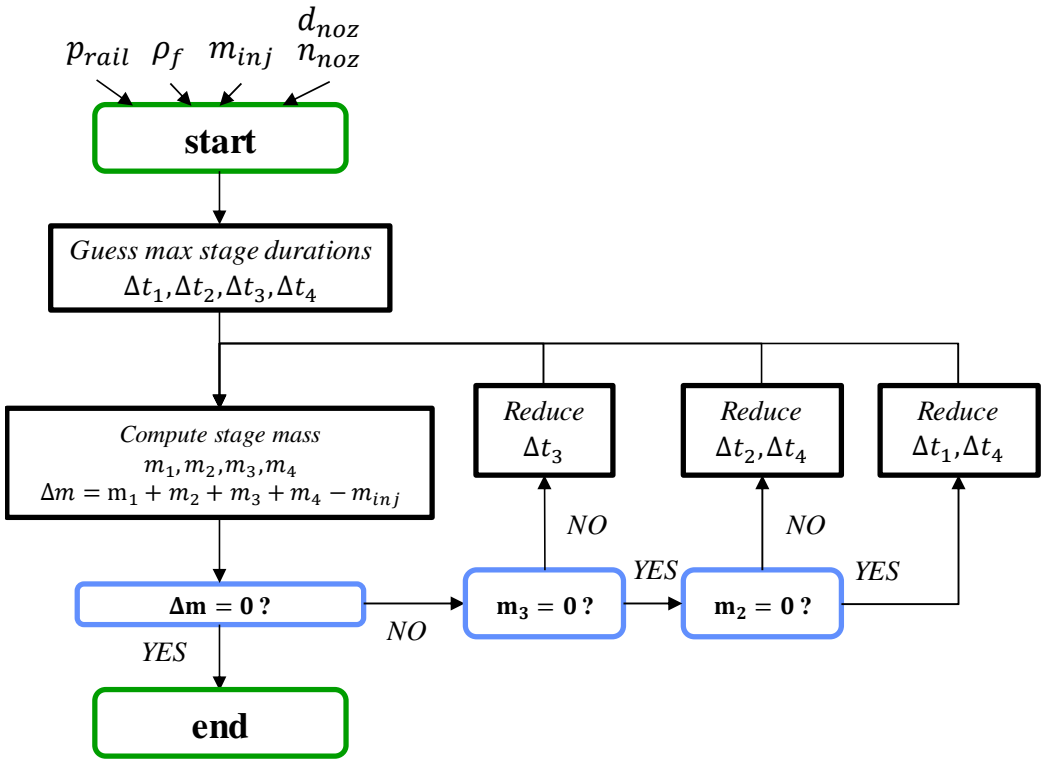

Figure 2. Flow-chart of the computational procedure for matching the desired injected mass.

First, mass is removed from the steady-state stage 3, until this stage is eventually completely removed from the injection rate. Then, additional mass has to be simultaneously removed from both one opening stage (2 and, later, 1) and from the descent stage. During stage 2, one must remove a trapezoidal area from the injection profile, such that flow velocities at the end of stage 2 and at the beginning of stage 4 match. The same strategy applies when the injection becomes short enough, that also stage 2 is removed from the rate profile. In between iterations, the injection rate profile is also smoothed using a floating average method to produce rounded corners between stages.

Experiments and Model calibration

Polynomial coefficients for a CRI2.2 injector platform were obtained from experimental measurements performed on the same injector platform, in facilities at the Sandia National Laboratories and at the University of Wisconsin. It should be noted that the same calibration procedure can be applied to any other high-pressure injection systems, provided that enough experimental data is available. The simple 0D Bernoulli flow model provides accurate maximum flow estimates, while platform-specific calibration is needed to accurately capture opening and closure transients, which mostly affect short injection events (i.e., pilot injections). During the transients, injection pressure is the most relevant parameter; hence, suitable calibration data should include enough pressure-range points to enable reliable estimation of the polynomial expansions: $u_{inj}(p_{rail}, dt_1)$, $a_2(p_{rail})$, $a_4(p_{rail})$.

A summary of the fuels and injection quantities employed during the campaigns is reported in Table 2. Measurements of partially-premixed combustion (PPC) and pilot injection rates at Sandia used a Moehwald HDA injector characterization device [24]. Both PPC and pilot injection rates reproduced experimental conditions in a light-duty research optical diesel engine [25, 23]. The experiments used three rail pressures (p_{rail} = *500, 860, 1220 bar*), two chamber pressures (p_{back} = *41, 56 bar*), and two signal conditioning filters. The digital filtering was done with raised cosine FIR filters with two different

roll-off factors and cutoff frequencies: 10 kHz / 0.5 and 6.0 kHz / 0.8 [24]. For each condition, the injection duration was adjusted to obtain the desired injected quantities. Small differences were observed between measured injection rates with different chamber backpressures; for the lower pressure, some problems were also encountered at 1220 bar rail pressure, probably related to excessive cavitation or pressure oscillations in the chamber with the low-viscosity fuel. PPC injection rates were also measured at the University of Wisconsin using a Bosch rate of injection (ROI) meter [26], and employing a CN=47.7 certification US diesel fuel.

Ensemble-averaged measured injection rate laws are reported later in Figures 6,7,8 for the pilot injections, and Figures , for the PPC injections. The injectors employed in the two institutions were not identical, though they were the same model. Even though the line lengths between the rails and injectors may have been different, and the fuel employed was not the same (certification diesel vs. PRF25), the rates reported in Figures 9 and 10 are remarkably similar. We assumed these differences can be regarded as a measure of the uncertainty in the injection rate profile, such that an injection rate model can capture an "average" pulse suitable for engine simulations, and we later investigated the impact of this uncertainty on the mixture formation process. Fluctuations at the tail of the injection rate which may be due to needle closing or pressure oscillations and likely cause fuel dribble, were not considered.

Model coefficient calibration. Polynomial fits to the model's calibrated constants were obtained from observed quantities in the whole set of experimental measurements, made up of a total of 20 experimental points sampled from the experimental injection traces.

Experiment	PPC injection, PRF25	pilot injections, DPRF58	PPC injection, di#2
Facility	Sandia	Sandia	UW
Fuel	75% n-heptane 25% iso-octane	42% $nC_{16}H_{34}$ 58% iso-$C_{16}H_{34}$	Certification US diesel fuel, CN=47.7
Injection measurement device	Moehwald HDA		Bosch ROI meter [26]
Injected mass	8.8 mg	1, 2, 3, 4 mg	5.9, 6.9, 8.8 mg
Injection pressure	500 bar 860 bar 1220 bar	500 bar 860 bar	500 bar 860 bar 900 bar 1000 bar 1100 bar

Table 2. Summary of the experimental measurements employed to calibrate the injector model.

Stage 1 was calibrated using the peak velocity at maximum needle lift time, as reported in Figure 8. According to the experiments, this duration is approximately constant and was assumed to occur at $t_1 = 0.1ms$. A quadratic polynomial was employed for estimating the dependency of the peak velocity with respect to rail pressure, as reported in Figure 3. Observed peak velocities during short, pilot

injection pulses exhibited slightly higher values than those of longer, PPC injection pulses, likely due to inertial flow effects. The polynomial fit led to an almost linear relationship with rail pressure. Stage 2 slope coefficient data is reported in Figure 4. Here, quadratic dependency on rail pressure was more evident, and it was again modeled using a second-degree polynomial. Again, slightly lower slope coefficients were observed for all PPC injections, though their behavior was less distinct from that of pilot injections as in stage 1. Finally, stage 4 (needle descent) slope data is reported in Figure 5. During stage 4, the needle valve closes, and the injection velocity decrease is dominated by the interaction between the spring force and viscous forces in the fuel stream. PPC injections with certification diesel fuel exhibited smaller descent rates and longer overall descent

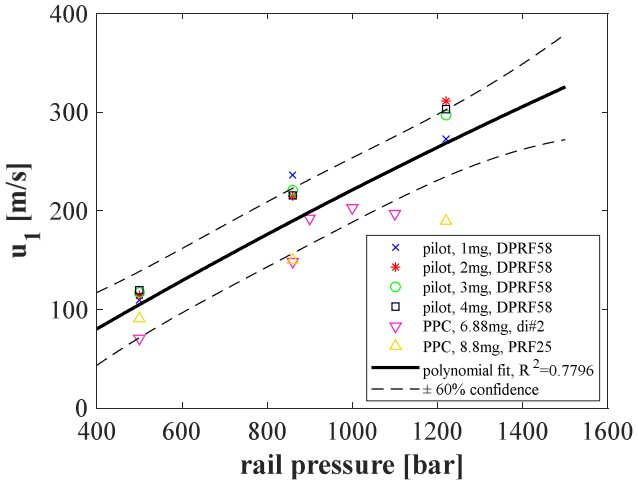

Figure 3. Polynomial fit for stage 1 maximum velocity. Dashed lines represent a ±60% confidence interval of the polynomial fit.

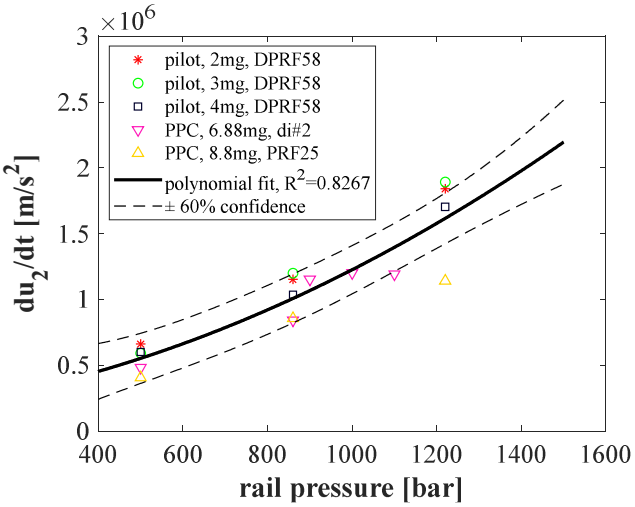

Figure 4. Polynomial fit for stage 2 velocity increase slope. Dashed lines represent a ±60% confidence interval of the polynomial fit.

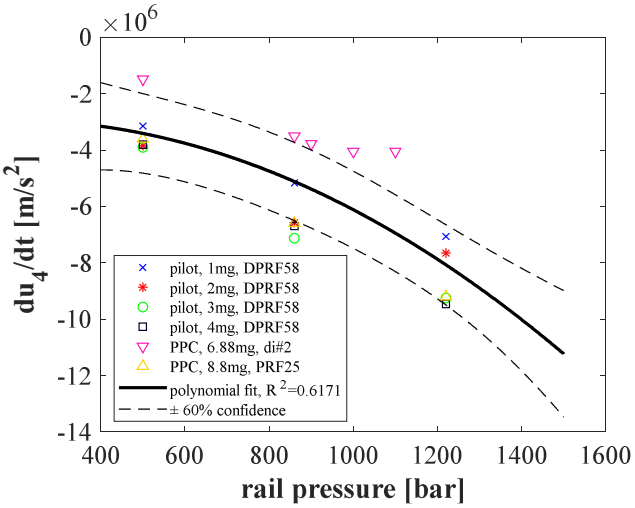

Figure 5. Polynomial fit for stage 4 descent velocity slope. Dashed lines represent a ±60% confidence interval of the polynomial fit.

duration. Differences in fuel physical properties were ruled out as potential causes for this behavior, as DPRF58 fuel, which exhibited among the fastest descent rates at any injection pressures, has very similar transport properties (density, molecular viscosity, surface tension) to certification diesel fuel **[25]**. Overall r-squared values between 0.61 and 0.83 were observed; closest behavior to the polynomial was observed for the stage-2 hydraulic transient coefficient, while most deviation was observed for the end-of-injection stage 4 descent slope, which is also affected by significant signal oscillations in the observed experimental traces.

Results and discussion

Injector model validation

The injector model was first validated against the measured injection rates from the experimental campaigns employed for the calibration. All validation cases were setup using common rail pressure

and total injected mass from the corresponding experimental measurements. Figures 6,7,8 report validation for the pilot injections at rail pressures of 500, 860 and 1220 bar, respectively. A satisfactory agreement was obtained for all injected mass values, 1 to 4 mg, and all three rail pressures. In all cases, both total injection duration and rate of velocity descent during needle closure were very well captured. The needle-opening-stage exhibited in the experiments some slight differences among the injected mass values, likely due to inertial effects, that could not be captured by the model. As a result, the 1mg injection rate laws slightly under-estimated peak injection velocity.

Figure 9 shows model validation for PPC injections with certification diesel fuel. Slopes of both the opening stage and the full-lift hydraulic transient are well captured; descent slopes are slightly over-estimated, as also highlighted in Figure 5. The overall injection durations were acceptable, even if the model predicted slightly shorter total injection times, and slightly higher peak mass flow rates. Figure 10 shows validation for PPC injections from the Sandia campaign, with similar injected mass but DPRF58 fuel. Again, modeled injection rate laws exhibited slightly shorter total injection times than those measured, caused by larger peak mass flow rates. Also, the simple model does not capture some of the local wobbling behavior of the injection rate law during the hydraulic transient stage measured at this experimental facility.

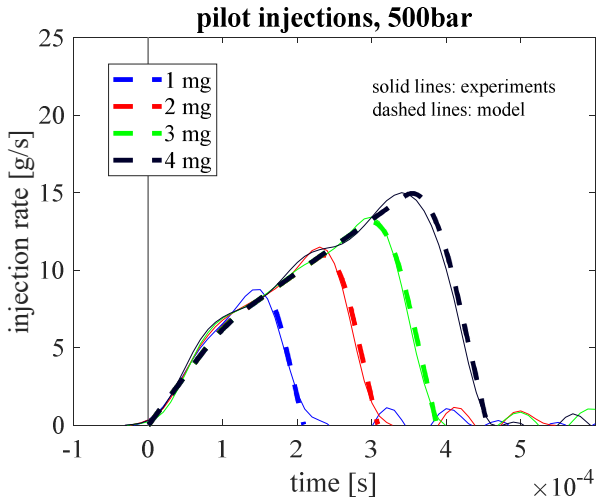

Figure 6. Model validation. Pilot injections, DPRF58, p_{inj}=500bar. Solid lines: experimental results [24]; dashed lines: model predictions.

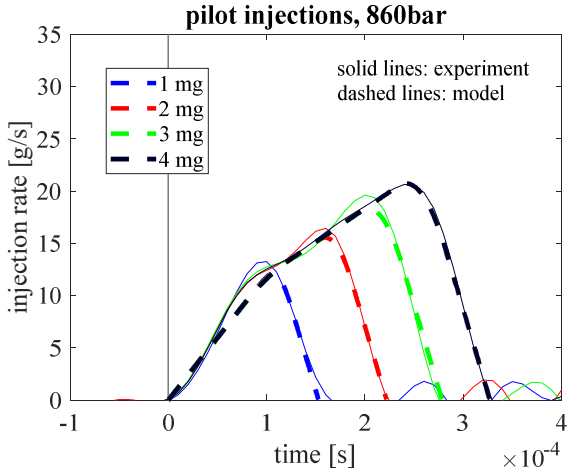

Figure 7. Model validation. Pilot injections, DPRF58, p_{inj}=*860bar*. Solid lines: experimental results [24]; dashed lines: model predictions.

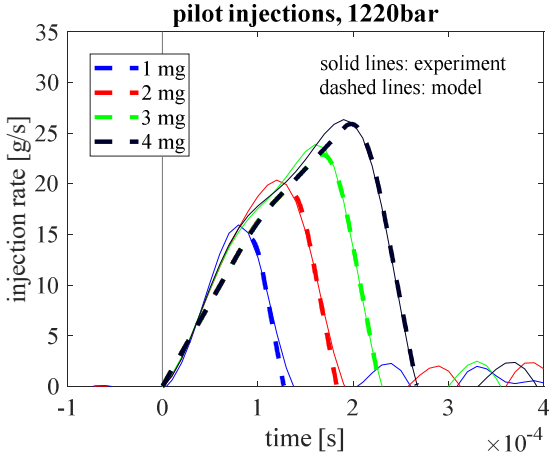

Figure 8. Model validation. Pilot injections, DPRF58, p_{inj}=*1220bar*. Solid lines: experimental results [24]; dashed lines: model predictions.

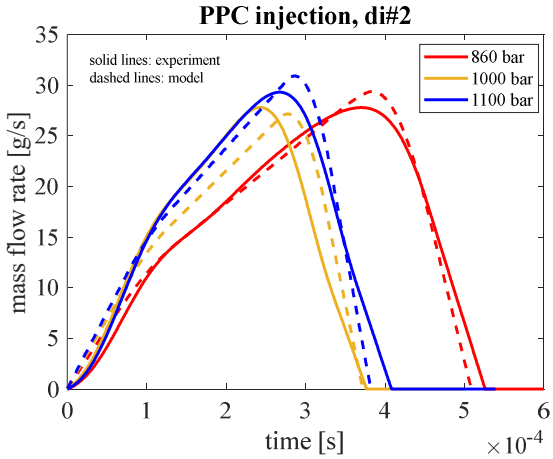

Figure 9. Model validation. PPC injections, US #2 diesel fuel, pinj=860, 1000, 1100 bar. Solid lines: experimental results [27]; dashed lines: model predictions.

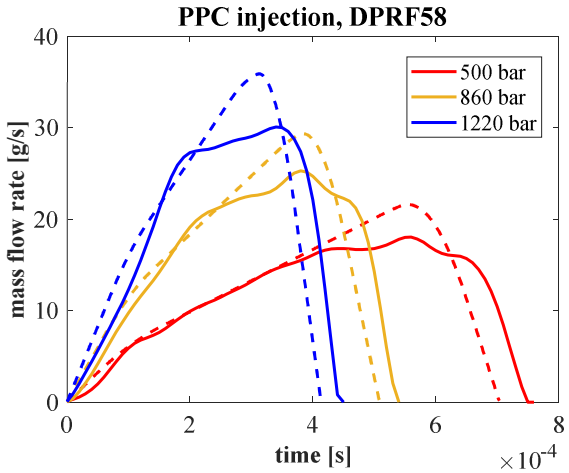

Figure 10. Model validation. PPC injections, DPRF58 fuel, p_{inj}=*500, 860, 1220 bar*. Solid lines: experimental results **[24]**; dashed lines: model predictions.

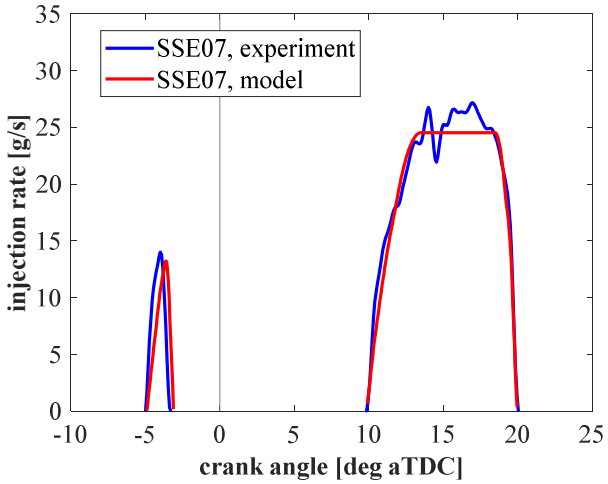

Figure 11. Model validation. CDC pilot+main injection strategy (SSE_{pilot} = *-7 deg aTDC*), DPRF58 fuel, p_{inj}=*1100 bar*.

PPC injection pulses are inherently transient, as injected mass is large enough to inject all fuel as a single pulse, but not enough to achieve steady-state open injector mass flow. As the relative importance of the transients and their inherent rail pressure oscillations is increased, model accuracy is more affected. Note that the same consideration also applies to the experiments: as the coefficient fits of Figures 3,4,5 also show (pink downward-looking triangles), experimental data for the PPC injections from this campaign is at the edges of the confidence bounds.

Predicted and measured injection rates from a conventional diesel combustion (CDC) operating condition in a 1.9L optically accessible engine [28] were also compared. The injection features a split pilot+main pulse strategy, with rail operated at p_{rail}=*1100bar*, employed for a part-load (9bar IMEP) operating point. Start of solenoid energizing (SSE) timing for the pilot injection is SSE=-7 deg aTDC, and the main injection pulse starts at approximately 9.1 CA deg aTDC [29]. Injection rates are represented in Figure 11. Both the pilot and main injection pulses were well captured. The pilot injection had acceptable peak velocity and duration. The main injection pulse exhibited accurate total

pulse duration, and both opening and closing velocity slopes were well predicted. The steady-state part of the injection also averaged the experimental trace well, though it does not predict its oscillations around the average value.

Model sensitivity with respect to the two input parameters, injected mass and rail pressure, and the calibration coefficients, was also assessed. Figure 12 shows predicted injection rate laws from an injected mass sweep from $m_{inj}=1mg$ (pilot injection) to $m_{inj}=28mg$ (long main injection). For any injected mass, the model dependency on rail pressure is unvaried. Hence, transient velocity slopes as well as peak injection velocity do not change. The plot highlights the model's staged-law behavior: the longest injections feature all 4 injection stages; as the injected mass is reduced, the steady-state part is accordingly shortened, until it eventually disappears. The shortest injection pulses only have either stages 1-2-4, or 1-4 only. Figure 13 shows model sensitivity to injection pressure instead. Here, total injected mass $m_{inj} = 8.8mg$ was held constant, and rail pressure was varied from $p_{rail}=500bar$ to $p_{rail}=2000bar$. Note that both the upper pressures were extrapolations from the calibration range. With increasing rail pressure, the magnitude of all slopes increases, yielding shorter and faster stages, which also make the whole injection pulse duration shorter. At this PPC-like injected mass value, the steady-state stage is only reached for the peak rail pressure $p_{rail}=2000\ bar$.

Figure 14 reports model sensitivity when perturbing the calibration coefficients. For a range of injection rail pressures and pulse mass, the sensitivity of total injection duration was analyzed by computing finite-difference approximations with perturbations of coefficients c_1, a_2, a_4. The sensitivities are expressed as percent change in total injection duration per percent-confidence-change in each parameter, i.e., with respect to a finite step corresponding to a ±1% of that variable's fit confidence interval at the given injection pressure (see Figures 3, 4, 5). The opening transient speed coefficient c_1 has the greatest impact overall, as its 1% increase from the standard fit led to a reduction in total injection time from 5% to more than 25% overall, the impact being stronger for those pilot injections where near-steady-state injector opening is almost never experienced. The same behavior, with significantly smaller extent, was observed for the closing transient constant a_4. A faster closing transient still leads to a shorter injection, but with lesser extent, and with a less straightforward dependency on injection pressure and mass. Sensitivity to coefficient a_2 exposed the most complex behavior: at fixed injection pressure, the injection time reduction has a maximum per injected mass between 7 and 8 mg. In fact, at lower injected mass, the duration of the hydraulic transient is short, and it may even disappear if the mass is low enough. In longer pulses, instead, a faster hydraulic transient will cause some reduction of the injection time, but its relevance will be reduced the longer the injection, where a possibly long fully-open steady-state stage will be present.

Figure 15 reports how the injection rate prediction for the pilot+main strategy of Figure 11 changes when altering the polynomial coefficients by ±60% of the confidence band. The pilot injection experiences greater shape change, with different total duration and peak injection mass flow rate. The long pulse has similar peak injection velocity, but its time span is changed as faster or slower opening and closing transients take place. As the sensitivity study showed, the relative difference is much greater for a low injection pressure of 750 bar: also the main injection is much longer, with a

more than doubled opening transient time, only partially compensated for by a shorter duration of the fully-open needle stage.

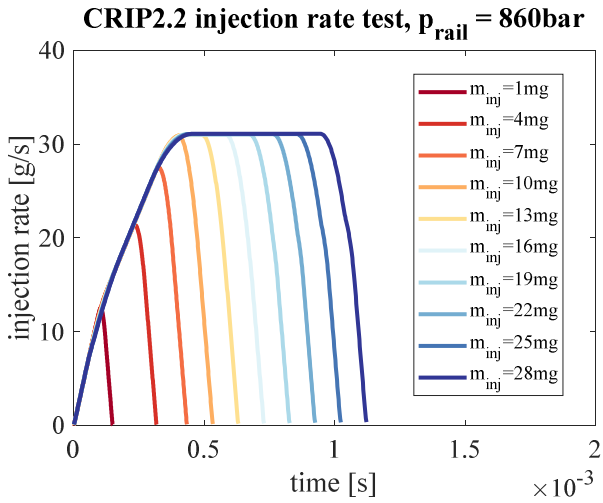

Figure 12. Model sensitivity to injected mass.

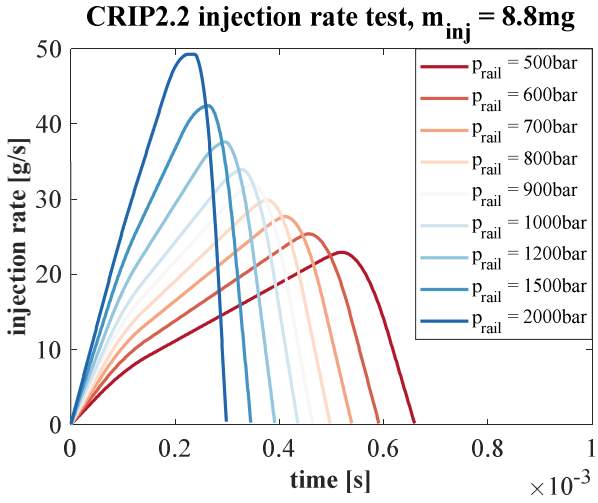

Figure 13. Model sensitivity to rail pressure.

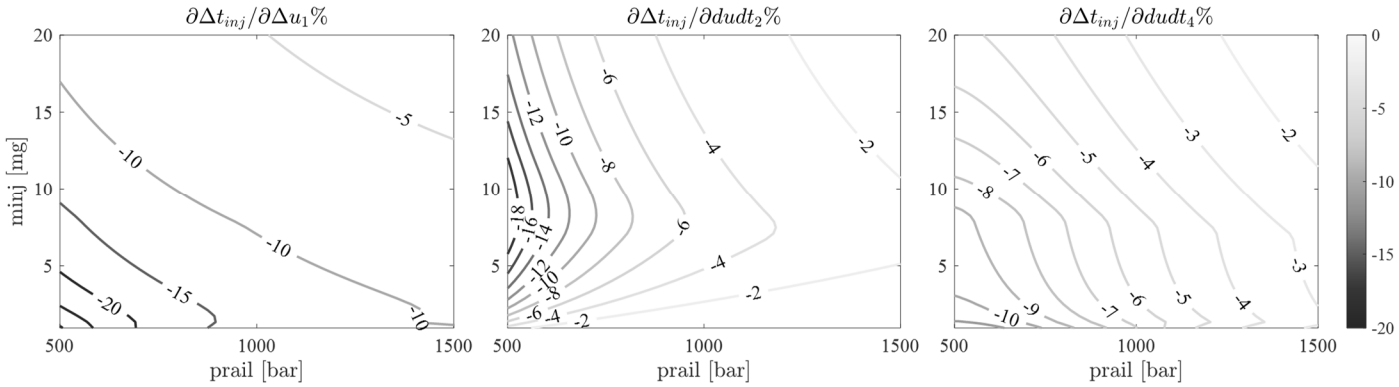

Figure 14. Sensitivity of predicted injection duration (as percent of baseline fit duration) with respect to perturbations in polynomial coefficients (left) c_1, (center) a_2, (right) a_4 (as percent of the fit's confidence range).

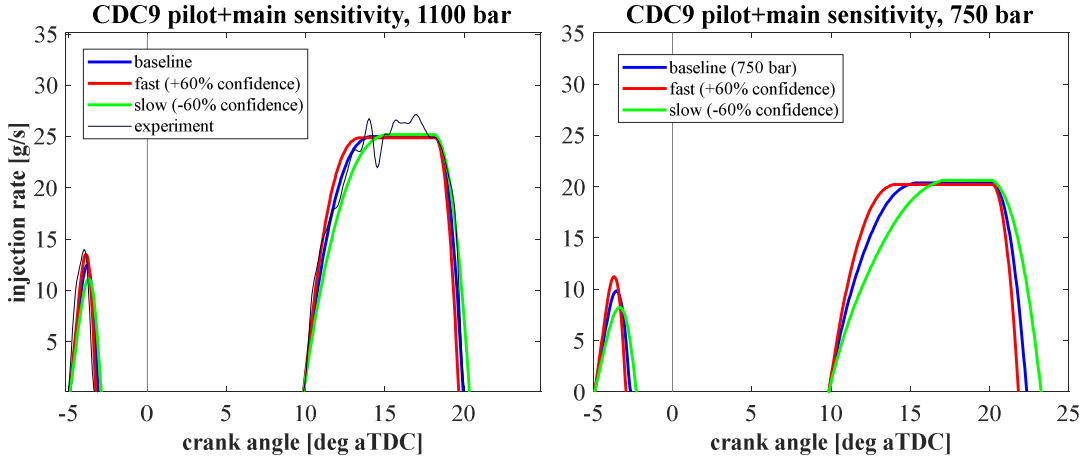

Figure 15. Sensitivity of the CDC9 pilot+main strategy to a change of polynomial coefficient estimates corresponding to ±60% of the fitting confidence values. (left) *p_{inj}=1100 bar* experiment; (right) *p_{inj}=750 bar* exercise.

Application to diesel engine modeling

The experimental studies of detailed local equivalence ratios by Sahoo et al. [30, 31] were adopted to validate the injector model presented in this work for usage with internal combustion engine simulations. The injector model was coupled with the FRESCO CFD platform to validate mixture formation predictions in light-duty diesel engine calculations. Measurements were made on a single-cylinder, optically accessible diesel engine, derived from a production GM four cylinder 1.9L light duty engine platform. The research engine, as represented in Figure 16, was equipped with a fused-silica piston having full geometrical details, including valve recesses. A full description of the experimental engine and injection system setup can be found in [31], while a summary of the main engine details is also reported in Table 3.

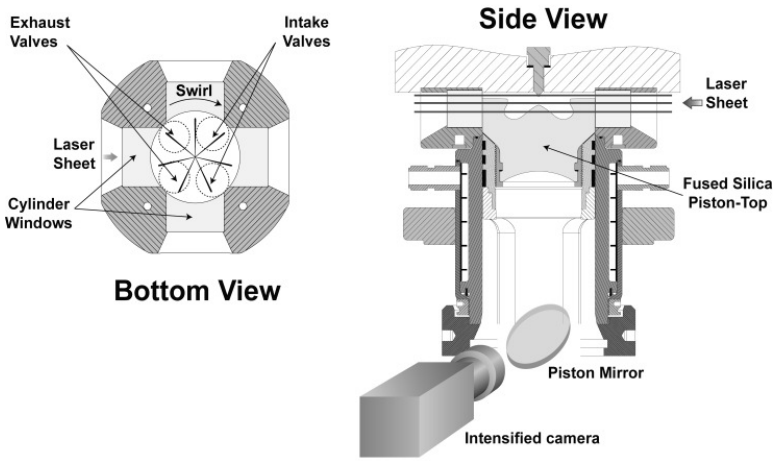

Figure 16. Schematic representing the optical access engine setup, including laser sheet locations and camera viewing direction.

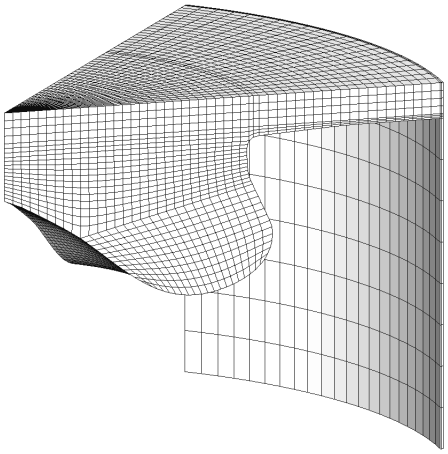

Figure 17. View of the 1.9L engine computational grid close to TDC.

Engine specifications

Bore x stroke [mm]	82.0 x 90.4
Unit displacement [cm^3]	477.2
Compression ratio	16.38 : 1
Squish height at TDC [mm]	0.88
Swirl ratio [-]	2.2

Operating condition details

Injection strategy	PPC	pilot
Fuel composition [mole fr.]	75% nC_7H_{16}	42% $nC_{16}H_{34}$
	25% iC_8H_{18}	58% i-$C_{16}H_{34}$
Fluorescent tracer [mass fr.]	0.5% C_7H_8	0.5% $C_{11}H_{10}$
Equivalent Cetane Number	47	50.7
Intake charge composition	100% N_2	
Intake pressure [bar]	1.5	
Intake temperature [K]	300	381
Engine speed [rpm]	1500	
IMEP [bar] (reacting)	3.0	---
Injected fuel mass [mg]	8.8	1, 2, 3, 4
Start of Injection [deg]	-23.0	-15.0
Injection pressure p_{rail} [bar]	860 (Fig. **Error! Reference source not found.**)	500, 860 (Fig. 6, 7)

Table 3. Operating conditions details for both the PPC-like and the pilot injection experiments in the 1.9L engine.

Local equivalence ratios were measured with the Planar Laser-Induced Fluorescence (PLIF) method in a non-reacting charge of pure nitrogen, with similar near-TDC density as the reference combusting conditions [27]. Three horizontal plane locations were imaged, as represented in Figure 16: P1 bisected the squish volume height; P2 at the piston bowl rim edge, and P3 deep into the piston bowl, at its maximum radial extent [31]. A comparison of the two baseline operating conditions is reported in Table 3.

The FRESCO CFD simulation platform was used for this study. [32]. The generalized re-normalization group (GRNG) k-epsilon turbulence model was used [33]. Fuel injection and spray phenomena are modeled with an enhanced Lagrangian-Droplet/Eulerian-Fluid (LDEF) approach [13], with optimized model constants against Engine Combustion Network data [34]. No further tuning was performed for the current study, as comparisons with experimental liquid and fuel vapor data were in good agreement [35].

PPC mixture formation. Partially Premixed Combustion (PPC)-like injections operated a short single-pulse, near-TDC injection targeting the piston bowl rim, designed for high EGR ratio, (10% oxygen volume fraction), and a swirl ratio Rs = 2.20. Figure 18 shows experimental versus numerical comparisons of local equivalence ratio for a p_{rail} = 1220bar injection at the three experimental planes and at three crank angles: -15.0, -10.0 and -5.0 crank angle degrees aTDC. It should be noted that this injection pressure is closer to values at which the spray models and their constants have been validated. The computational model does a satisfactory job at predicting the overall equivalence distribution in the combustion chamber.

In the squish plane (Figure 18 left), fuel vapor penetration into the squish region is correctly predicted at all three crank angles. At -15.0 aTDC, rich pockets have reached the squish volume and are radially centered in the outer annular region, while near-stoichiometric jet tails are still floating in the central part of the cylinder. At -10 deg aTDC, the rich pockets have stretched out until the liner, but peak equivalence ratios are lower as a result of swirl mixing. At -5 deg aTDC, a similar distribution, with lower peak values and more blurred, is seen.

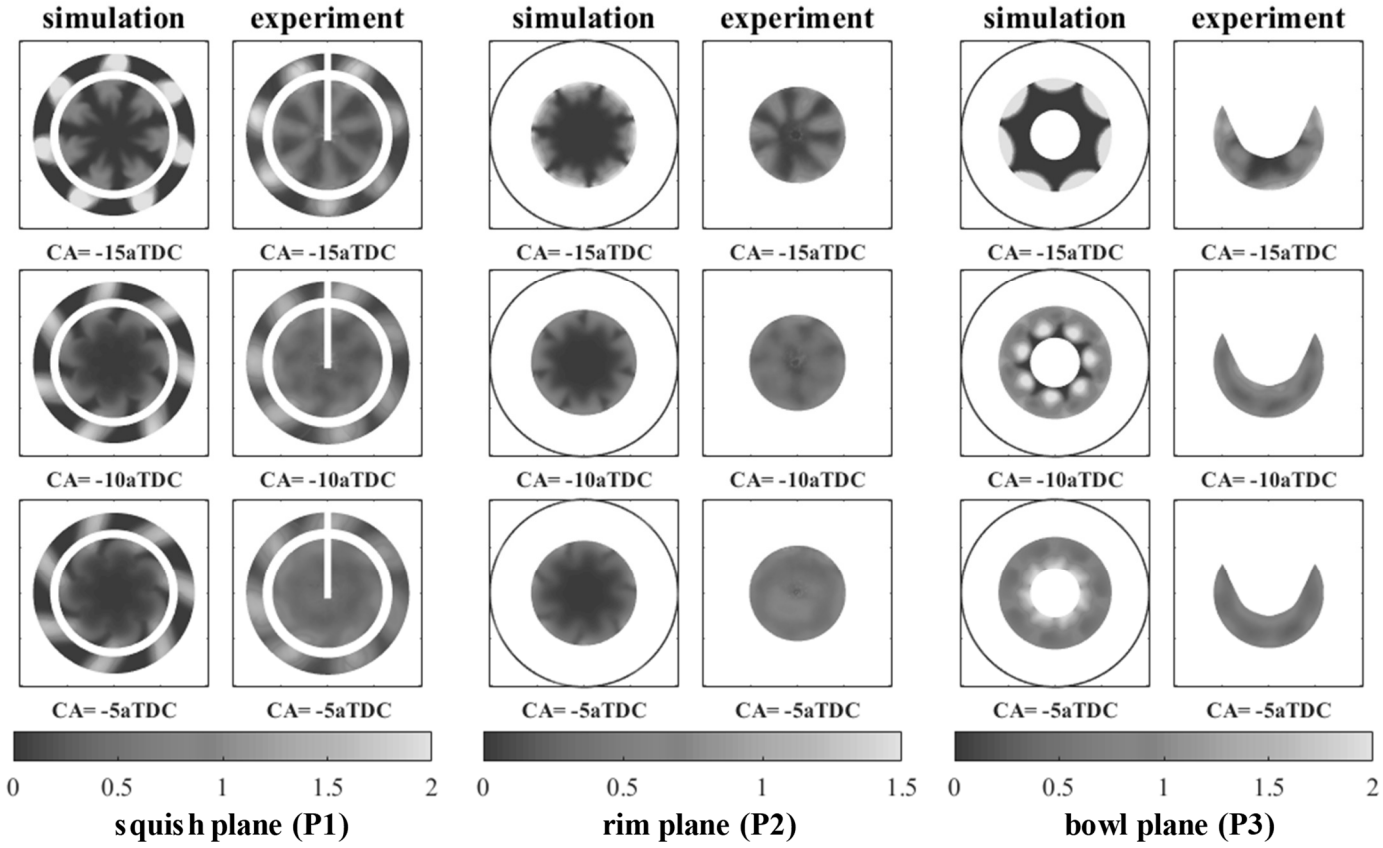

Figure 18. Numerical vs. experimental equivalence ratio distribution comparison for the PPC case,

plane P1 (left, squish), P2 (center, bowl rim), P3 (right, deep bowl). Regions of missing/unreliable signal from PLIF reproduced according to [31].

The bowl rim plane comparisons of Figure 18 (center) highlight jet targeting. Shortly after the end of injection, stagnation pockets survive close to the bowl rim with high equivalence ratio, while the jet tails are disappearing behind. The experimental images have a shorter field of view due to warping at the rim, and a few millimeters closest to it are not visible. The leaning effects of mixing are seen in the latter crank angles. Bowl plane measurements in Figure 18 (right) highlight the model capability to predict appropriate travel along the bowl surface and back towards the center of the cylinder. The simulation correctly shows fuel to appear at -15 deg aTDC on the outer surface (due to fuel jet splitting at the rim); fuel footprints correctly appear back along the inner bowl surface, close to the center of the cylinder, at 10 deg aTDC. Full 360-degree spreading at -5 deg aTDC is seen too. Slightly high peak equivalence ratio predictions can be accepted, as the sector mesh approach is known to under-predict both local turbulence [28, 36].

Pilot injection mixture formation. Pilot injection experiments [30] had the same engine speed of 1500 rev/min, with near-TDC ambient density of 19.6 kg/m^3. Start of injection (SOI) was held at 15 deg bTDC, to avoid the impact of spray targeting and transients in in-cylinder flow and thermodynamics on mixture formation. A binary fuel Diesel Primary Reference Fuel mixture (DPRF58), with 42% n-hexadecane and 58% 2,2,4,4,6,8,8-heptamethylnonane by volume was used. Figure 19 represents compares predicted with experimental equivalence ratio distribution at the measurement planes for a rail pressure p_{rail} = *860bar*. Also, the model is compared with a simpler ROI approach which features a constant injection velocity, and same injection duration as predicted by the current model. Comparing CFD with in-cylinder is no trivial task, as optical thickness of the laser sheet, scattering due to liquid fuel, significant background reflection from the cylinder head and valves affect the comparison. Still, the current model appropriately captures higher equivalence ratios close to the rim for plane P2, and closer to the center for P1; the current model also captures the bi-modal distribution in P1 at the latest crank angles, which is instead failed by the simpler ROI model.

The effects of rail pressure on mixture formation were also analyzed. Figure 20 (left) shows numerical versus experimental comparisons of in-cylinder equivalence ratios for the same rail pressure. In the squish plane of Figure 20, early pilot injections still have a plume-like shape, different from fully-developed diesel flame, shortly after EOI. At -6 deg aTDC, small stagnation regions have formed at the rim; their equivalence ratio is lean, as seen in the experiments. Close to TDC, similar radial extent is seen, with some additional swirling. No penetration into the outer squish volume, or in the deep bowl plane, is observed. Figure 19 (right) shows equivalence ratios at the bowl rim plane: here, the same stagnation regions are seen.

In Figure 21, a lower rail pressure prail = 500bar was employed. Compared to the previous, slower penetration is seen. Fuel in the squish plane (Figure 21) is only seen in the central part of the cylinder, corresponding to the injected jet structure, while fuel at the bowl rim is hardly seen, suggesting very little penetration after the impact towards the squish. In plane P2, similar penetration is instead seen as for the higher rail pressure, but with slightly delayed timing, as shown by the smaller equivalence ratios of the 12 deg aTDC image. Overall, the simulation correctly predicted the changes in spray pattern due to operation with a lower rail pressure: delayed impact with the bowl rim and shorter penetration with smaller equivalence ratios were seen.

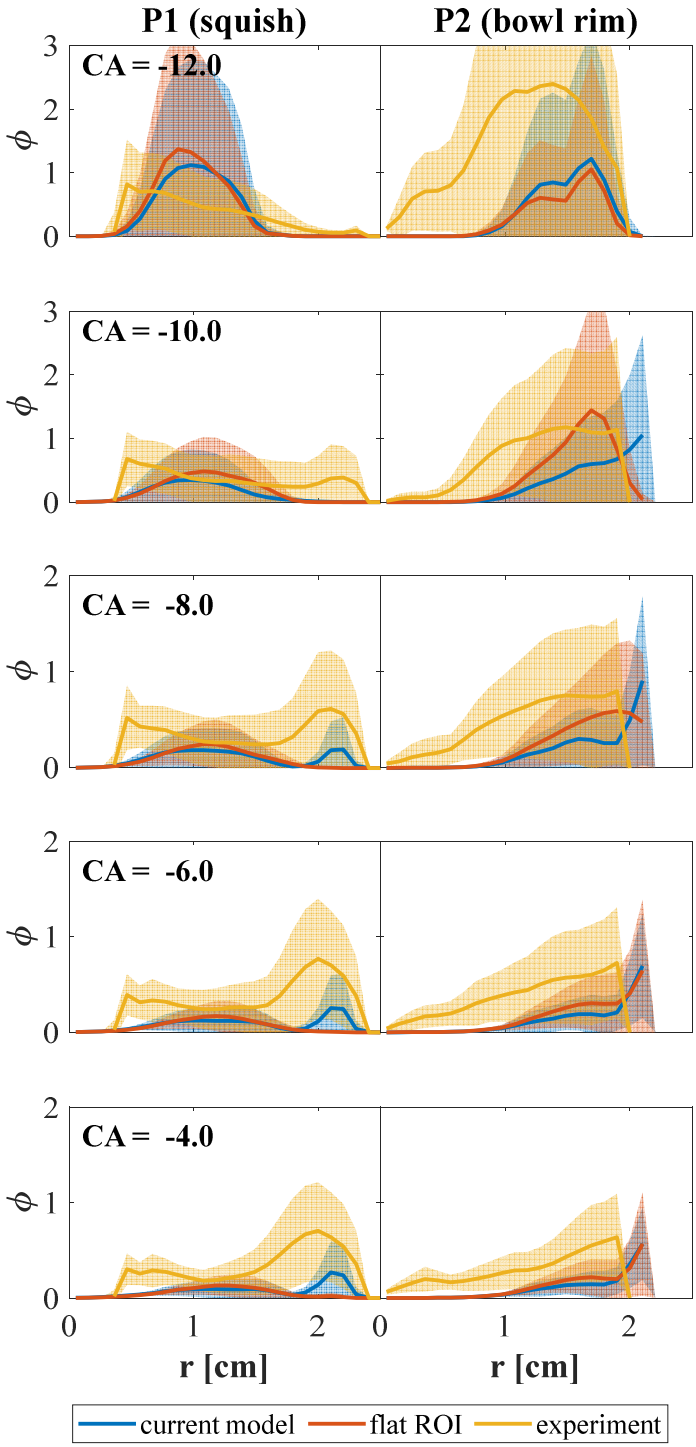

Figure 19. Predicted vs. measured planar equivalence ratio distributions versus cylinder radius for a 4 mg pilot injection, p_{rail} = *860 bar*. Left: plane P1 (squish); right: plane P2 (bowl rim). Solid lines represent the azimuthal mean; shaded areas represent a ± one standard deviation of the azimuthal distribution.

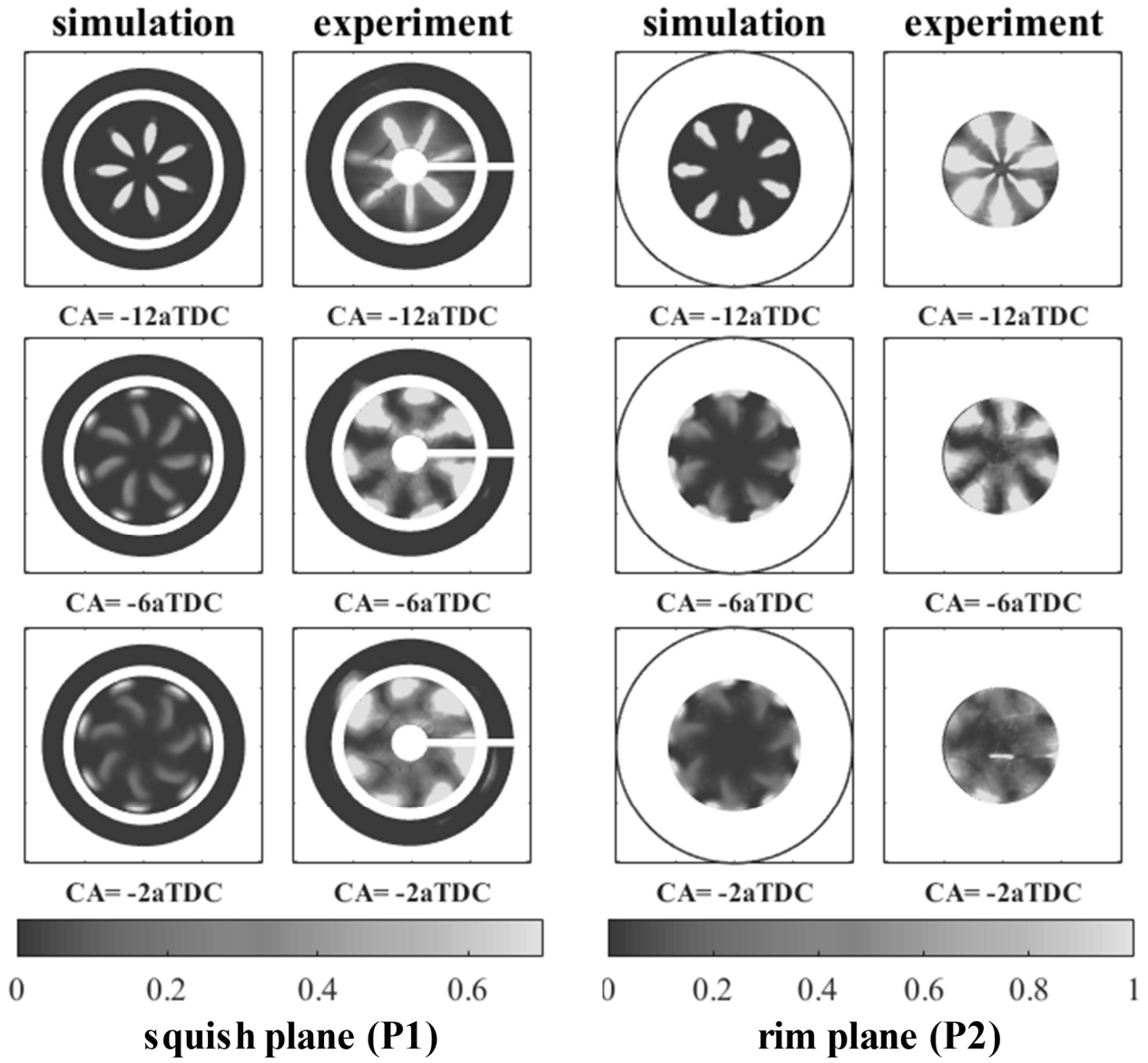

Figure 20. Numerical vs. experimental equivalence ratio distribution comparison for a 4 mg pilot injection, p_{rail} = *860 bar*. Left: plane P1 (squish); right: plane P2 (bowl rim).

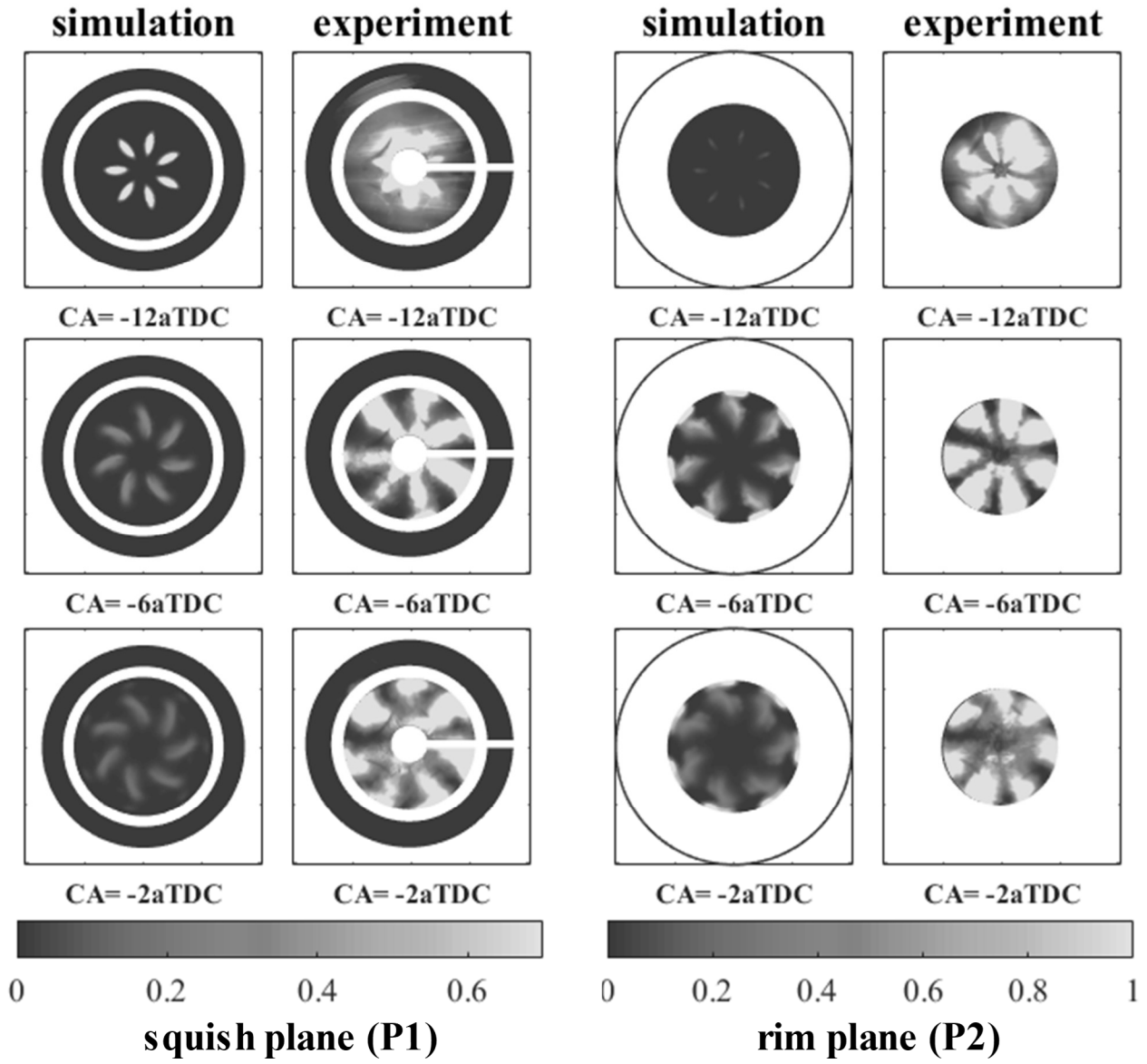

Figure 21. Numerical vs. experimental equivalence ratio distribution comparison for a 4 mg pilot injection, p_{rail} = *500 bar*. Left: plane P1 (squish); right: plane P2 (bowl rim).

Concluding remarks

Injection rate modeling is of critical importance to capturing in-cylinder fuel-air mixture formation in internal combustion engines; yet, advanced injection rate prediction models require detailed information about the injector's inner geometry, mechanical and electrical structures, often unavailable to the engine modeler. In this paper, we developed a simple phenomenological injection rate model, which can be calibrated based on few available experimental injection rate measurements, easier to get either experimentally or in the literature. We calibrated and validated it for usage with the Bosch CRI2.2 injector, used in the Sandia Light-Duty diesel optical engine facility, part of the Engine Combustion Network. Then, we used it to generate injection rate input for engine CFD simulations, to model mixture formation in a light-duty diesel engine. The simulations repeatably produced reasonable predictions of fuel jet structure and in-cylinder equivalence ratio distributions from injection strategies for both partially-premixed combustion pilot injections.

Based on this study, the following conclusions could be drawn:

- The model only requires three tunable parameter fits, making it relatively easy to calibrate, and suitable to represent other injectors than the one employed in this work;
- Injection rate splitting into four separate stages allowed both fully-transient, short (pilot) injections and longer injections reaching steady-state operation to be accurately represented by the same model; such that also more complex strategies such as with both pilot and main pulses could be captured with both pulse duration and injection rate shape;
- The greatest deviations with respect to experimentally-measured injection rates were seen where also different experimental campaigns on the same injector platform exhibited noticeable discrepancies; this suggested that a simple model such as the one presented in this paper can be a suitable choice when it is impractical to manage uncertainties such as those from injector-to-injector geometry differences or from the experimental equipment;
- Once calibrated, the model produced acceptable quality results for a wide range of injected mass and rail pressure values. Appropriate injected mass dependency is attained as transient stages of the injection pulse are dynamically included or excluded from the injection rate based on the injected mass budget; rail pressure dependency is obtained by fitting the rate law parameters with rail-pressure-dependent polynomials;
- When employed for diesel engine modeling, accurate maps of in-cylinder mixture equivalence ratios could be obtained, demonstrating that the current model can be successfully employed for accurate, repeatable engine simulations.

References

[1] H. Zhao, Advanced Direct Injection Combustion Engine Technologies and Development. Volume I: Gasoline and Gas Engines, Woodhead Publishing, 2009.

[2] H. Zhao, Advanced Direct Injection Combustion Engine Technologies and Development. Volume II: Diesel Engines, Woodhead Publishing, 2009.

[3] A. Paykani, A.-H. Kakaee, P. Rahnama and R. D. Reitz, "Progress and recent trends in reactivity-controlled compression ignition engines," *International Journal of Engine Research,* vol. 17, no. 5, pp. 481-524, 2015.

[4] A. A. Amsden, P. J. O'Rourke and T. D. Butler, "KIVA-II: A Computer Program for Chemically Reactive Flows with Sprays," Los Alamos National Laboratories LA-11560-MS, Los Alamos, NM, 1989.

[5] D. L. Siebers, "Scaling Liquid-Phase Fuel Penetration in Diesel Sprays Based on Mixing-Limited Vaporization," *SAE Transactions Journal of Engines,* vol. 108, no. 3, pp. 703-728, 1999.

[6] D. Duke, A. Swantek, Z. Tilocco, A. Kastengren, K. Fezzaa, K. Neroorkar, M. Moulai, C. Powell and D. Schmidt, "X-ray Imaging of Cavitation in Diesel Injectors," *SAE International Journal of Engines,* vol. 7, no. 2, pp. 1003-1016, 2014.

[7] Z. Liu, k. Im, Y. Wang, K. Fezzaa, X. Xing-Bin, M.-C. Lai and J. Wang, "Near-Nozzle Structure of Diesel Sprays Affected by Internal Geometry of Injector Nozzle: Visualized by Single-Shot X-ray Imaging," in *SAE Technical Paper 2010-01-0877*, Detroit, 2010.

[8] A. I. Ramirez, S. Som, S. Aggarwal, A. L. Kastengren, E. M. El-Hannouny, D. E. Longman and C. F. Powell, "Quantitative X-ray measurements of high-pressure fuel sprays from a production heavy duty diesel injector," *Experiments in Fluids,* vol. 47, no. 1, pp. 119-134, 2009.

[9] K. E. Matusik, D. J. Duke, A. L. Kastengren, N. Sovis, A. B. Swantek and C. F. Powell, "High-resolution X-ray tomography of Engine Combustion Network diesel injectors," *International Journal of Engine Research,* vol. 19, no. 9, pp. 963-976, 2018.

[10] S. Moon, W. Huang, Z. Li and J. Wang, "End-of-injection fuel dribble of multi-hole diesel injector: Comprehensive investifation of phenomenon and discussion on control strategy," *Applied Energy,* vol. 179, no. 1, pp. 7-16, 2016.

[11] Q. Xue, M. Battistoni, D. E. Longman, S. P. Quan, E. Pomraning, P. K. Senecal, D. P. Schmidt, S. Som and C. F. Powell, "An Eulerian CFD model and X-ray radiography for coupled nozzle flow and spray in internal combustion engines," *International Journal of Multiphase Flow,* vol. 70, pp. 77-88, 2015.

[12] M. Vujanovic, Z. Petranovic, W. Edelbauer and N. Duic, "Modelling spray and combustion processes in diesel engine by using the coupled Eulerian-Eulerian and Eulerian-Lagrangian method," *Energy Conversion and Management,* vol. 125, no. 1, pp. 15-25, 2016.

[13] F. Perini and R. D. Reitz, "Improved atomization, collision and sub-grid scale momentum coupling models for transient vaporizing engine sprays," *International Journal of Multiphase Flows,* vol. 79, pp. 107-123, 2016.

[14] G. M. Bianchi, S. Falfari, M. Parotto and G. Osbat, "Advanced Modeling of Common Rail Injector Dynamics and Comparison with Experiments," *SAE Transactions Journal of Engines,* vol. 112, no. 3, pp. 55-72, 2003.

[15] R. Payri, J. Gimeno Garcia, R. Novella Rosa and G. C. Bracho Leon, "On the rate of injection modeling applied to direct injection compression ignition engines," *International Journal of Engine Research,* vol. 17, no. 10, pp. 1015-1030, 2016.

[16] R. Payri, G. Bracho, J. Gimeno and A. Bautista, "Rate of injection modelling for gasoline direct injectors," *Energy Conversion and Management,* vol. 166, pp. 424-432, 2018.

[17] J. A. Soriano, C. Mata, O. Armas and C. Avila, "A zero-dimensional model to simulate injection rate from first generation common rail injectors under thermodynamic diagnosis," *Energy,* vol. 158, pp. 845-858, 2018.

[18] L. Xu, X.-S. Bai, M. Jia, Y. Qian, X. Qiao and X. Lu, "Experimental and modeling study of liquid fuel injection and combustion in diesel engines with a common rail injection system," *Applied Energy,* vol. 230, pp. 287-304, 2018.

[19] G. M. Bianchi, S. Falfari, P. Pelloni, S.-C. Kong and R. D. Reitz, "Numerical Analysis of High-Pressure Fast-Response Common Rail Injector Dynamics," *SAE Transactions Journal of Engines,* vol. 111, no. 3, pp. 545-560, 2002.

[20] R. Payri, H. Climent, F. J. Salvador and A. G. Favennec, "Diesel injection system modelling. Methodology and application for a first-generation common rail system," *Proc. Instn. Mech. Engrs. Part D: J. Automobile Engineering,* vol. 218, pp. 81-91, 2004.

[21] R. Payri, S. Rubio, M. Aldaravi and J. Martinez Lopez, "Using one-dimensional modeling to analyse the influence of the use of biodiesels on the dynamic behavior of solenoid-operated injectors in common rail systems: Detailed injection system model," *Energy Conversion and Management,* vol. 54, no. 1, pp. 90-99, 2911.

[22] C. von Kuensberg Sarre, S.-C. Kong and R. D. Reitz, "Modeling the Effects of Injector Nozzle Geometry on Diesel Sprays," in *SAE Technical Paper 1999-01-0912*, Detroit, 1999.

[23] F. Perini, A. B. Dempsey, R. D. Reitz, D. Sahoo, B. Petersen and P. C. Miles, "A Computational Investigation of the Effects of Swirl Ratio and Injection Pressure on Mixture Preparation and Wall Heat Transfer in a Light-Duty Diesel Engine," in *SAE Technical Paper 2013-01-1105*, Detroit, MI, 2013.

[24] S. Busch and P. C. Miles, "Parametric Study of Injection Rates With Solenoid Injectors in an Injection Quantity and Rate Measuring Device," in *ASME Paper No. ICEF2014-5583*, Columbus, Indiana, USA, 2015.

[25] F. Perini, D. Sahoo, P. C. Miles and R. D. Reitz, "Modeling the Ignitability of a Pilot Injection for a Diesel Primary Reference Fuel: Impact of Injection Pressure, Ambient Temperature and Fuel Mass," *SAE Int. J. Fuels Lubr.,* vol. 7, pp. 48-64, 2014.

[26] G. R. Bower and D. E. Foster, "A Comparison of the Bosch and Zuech Rate of Injection Meters," in *SAE Technical Paper 910724*, Detroit, 1991.

[27] A. B. Dempsey, B. Wang, R. D. Reitz , B. Petersen, D. Sahoo and P. C. Miles, "Comparison of Quantitative In-Cylinder Equivalence Ratio Measurements with CFD Predictions for a Light Duty Low Temperature Combustion Diesel Engine," *SAE International Journal of Engines,* vol. 5, no. 2, 2012.

[28] F. Perini, S. Busch, E. Kurtz, A. Warey, R. C. Peterson and R. D. Reitz, "Limitations of Sector Mesh Geometry and Initial Conditions to Model Flow and Mixture Formation in Direct-Injection Diesel Engines," in *SAE Techical Paper 2019-01-0204*, Detroit, 2019.

[29] S. Busch, K. Zha, E. Kurtz, A. Warey and R. C. Peterson, "Experimental and Numerical Studies of Bowl Geometry Impacts on Thermal Efficiency in a Light-Duty Diesel Engine," in *SAE Technical Paper 2018-01-0228*, 2018.

[30] D. Sahoo, P. C. Miles, J. Trost and A. Leipertz, "The Impact of Fuel Mass, Injection Pressure, Ambient Temperature, and Swirl Ratio on the Mixture Preparation of a Pilot Injection," *SAE International Journal of Engines,* vol. 6, no. 3, pp. 1716-1730, 2013.

[31] D. Sahoo, B. Petersen and P. C. Miles, "The Impact of Swirl Ratio and Injection Pressure on Fuel-Air Mixing in a Light-Duty Diesel Engine," in *2012 Spring Technical Conference of the ASME Internal Combustion Engine Division*, Torino (Italy), 2012.

[32] F. Perini and R. D. Reitz, "FRESCO - an object-oriented, parallel platform for internal combustion engine simulations," in *28th International Multidimensional Engine Modeling User's Group Meeting at the SAE Congress*, Detroit, 2018.

[33] F. Perini, S. Busch, K. Zha and R. D. Reitz, "Comparison of Linear, Non-linear and Generalized RNG-based k-epsilon models for turbulent diesel engine flows," in *SAE Technical Paper 2017-01-0561*, Detroit, MI, 2017.

[34] "ECN Data Search Page," [Online]. Available: https://ecn.sandia.gov/ecn-data-search/. [Accessed 28 08 2018].

[35] S. Busch, "Light-Duty Diesel Combustion," in *DOE Vehicle Technologies Office and Hydrogen and Fuel Cells Program Annual Merit Review*, Washington, DC, 2017.

[36] F. Perini, P. C. Miles and R. D. Reitz, "A comprehensive modeling study of in-cylinder fluid flows in a high-swirl, light-duty optical diesel engine," *Computers & Fluids,* vol. 105, pp. 113-124, 2014.

[37] K. Zha, S. Busch, C. Park and P. C. Miles, "A novel method for correction of temporally- and spatially-variant optical distortion in planar particle image velocimetry," *Measurement Science and Technology,* vol. 27, p. 085201 (16 pp), 2016.

Acknowledgments

This work was performed under Sandia Subcontract 1890589, 1, sponsored by the United States Department of Energy, Office of Vehicle Technologies, with program managers Gupreet Singh and Michael Weismiller.

Sandia National Laboratories is a multi-mission laboratory managed and operated by National Technology and Engineering Solutions of Sandia, LLC., a wholly owned subsidiary of Honeywell International, Inc., for the U.S. Department of Energy's National Nuclear Security Administration under contract DE-NA-0003525. The views expressed in the article do not necessarily represent the views of the U.S. Department of Energy or the United States Government.

The authors also gratefully acknowledge Dr. Adam B. Dempsey from Caterpillar, Inc. for providing injection rate data on the CRI2.2 injector.